Supplementary information for:

Challenges in measuring sticky biogenic ice-nucleating macromolecules

Joseph Robinson[1], Martin I. Daily[1], Polly B. Foster[1], Jack P. Macklin[1], James B. McQuaid[1], Mark D. Tarn[1], and Benjamin J. Murray[1]

[1]Institute for Climate and Atmospheric Science, University of Leeds, UK

Data availability

The data associated with this publication is available at https://doi.org/10.5281/zenodo.19006498.

S1 Determining Average Handling Blanks for Wash-off and Drop-on Techniques

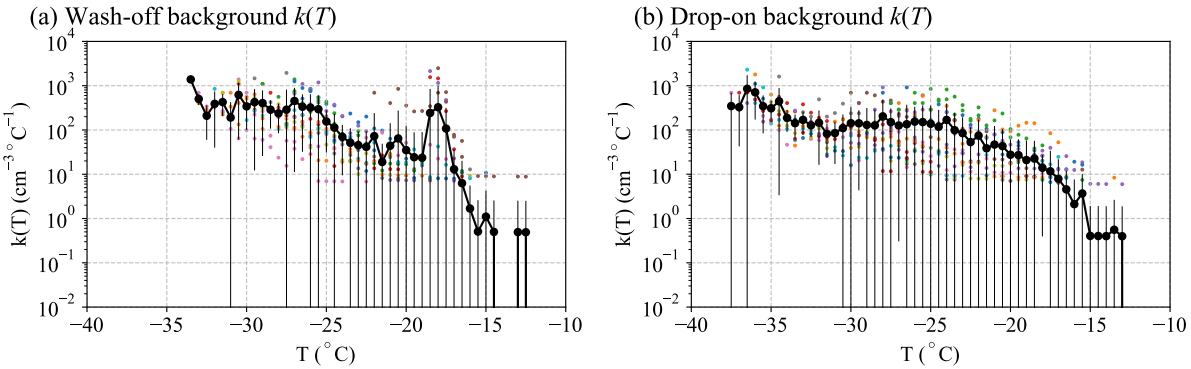

Figure S1: Differential freezing nucleus spectrum, $k(T)$, for the handling blanks for the (a) wash-off and (b) drop-on techniques. $k(T)$ was calculated for each handling blank and the average was found for each bin (including zeros) with the uncertainty being represented by the standard deviation.

Figure S1 shows the differential freezing nucleus spectrum, $k(T)$ data for the handling blank runs for the wash-off and drop-on techniques. For each handling blank, $k(T)$ was calculated in 0.5 °C temperature bins, and the mean and standard deviation were then calculated for each bin. These averaged backgrounds were used for all subsequent background subtraction steps for both filter techniques.

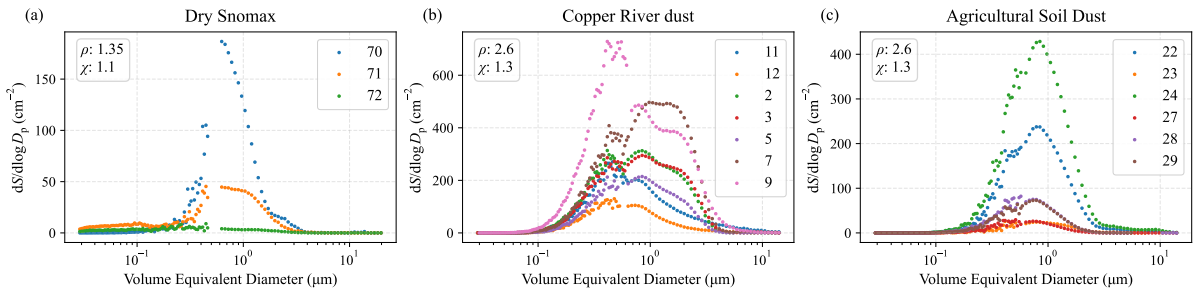

Figure S2: $\frac{\mathrm{d}S}{\mathrm{dlog}D_\mathrm{p}}$ size distributions for dry-dispersed samples from both the APS and SMPS data averaged over the experiment. The majority of the aerosol surface area is contributed to by particles near and above 1 μm, extending well into the supermicron range.

S2 Sampling Information and Individual Experiment Active Site Density Plots

The tables below (Table S2 to Table S8) summarise key parameters for each filter experiment, including sampling volume, average number concentration and surface area, their respective standard deviations (σ), and the peak diameter contributing to the surface area. Figure S2 and Figure S6 show the $\frac{\mathrm{d}S}{\mathrm{dlog}D_\mathrm{p}}$ size distributions for the dry- and wet-dispersed experiments, respectively. Figure S3 to Figure S5 show $n_\mathrm{s}(T)$ with associated uncertainties for the individual dry-dispersed experiments while Figure S7 to Figure S11 show $n_\mathrm{s}(T)$ with associated error for wet-dispersed experiments.

S2.1 Dry-Dispersed Samples

Table S1: Information about Dry Snomax Experiments.

ID	Date	Volume (L^{-1})	Number Conc. (cm^{-3})	Number Conc. σ (cm^{-3})	Surface Area ($\mu\mathrm{m}^2\mathrm{cm}^{-3}$)	Surface Area σ ($\mu\mathrm{m}^2\mathrm{cm}^{-3}$)	Peak Diameter (μm)
70	06/05/25	300	98.56	56.55	85.59	30.37	0.6
71	06/05/25	460	522.39	172.88	35.94	14.64	0.6
72	06/05/25	300	207.607	109.62	6.79	5.54	0.4

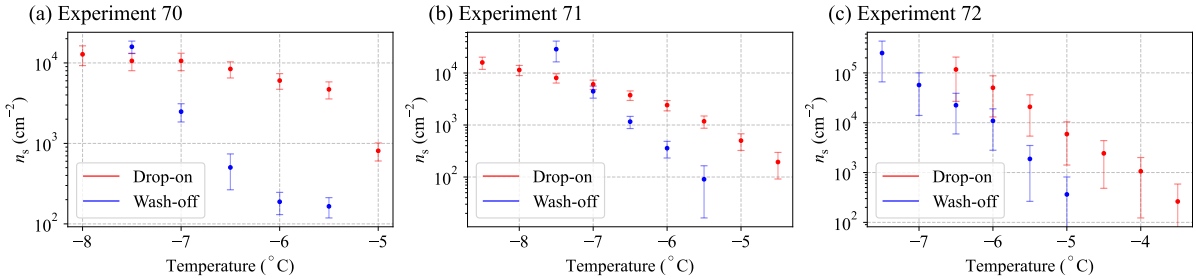

Figure S3: Active site density with error bars for all dry Snomax experiments.

Table S2: Information about Copper River dust Experiments.

ID	Date	Volume (L^{-1})	Number Conc. (cm^{-3})	Number Conc. σ (cm^{-3})	Surface Area ($\mu m^2 cm^{-3}$)	Surface Area σ ($\mu m^2 cm^{-3}$)	Peak Diameter (μm)
2	15/03/23	600	490.89	166.89	286.00	59.51	0.5
3	15/03/23	600	441.24	163.38	279.18	65.24	0.8
5	22/03/23	600	283.67	147.84	179.83	72.30	0.8
7	12/04/23	600	552.88	274.43	445.20	174.54	1
9	19/10/23	607.5	1097.00	333.20	566.18	170.04	0.5
11	30/10/23	600	405.76	510.06	194.92	247.43	0.4
12	30/10/23	600	210.89	129.30	89.72	47.82	0.5

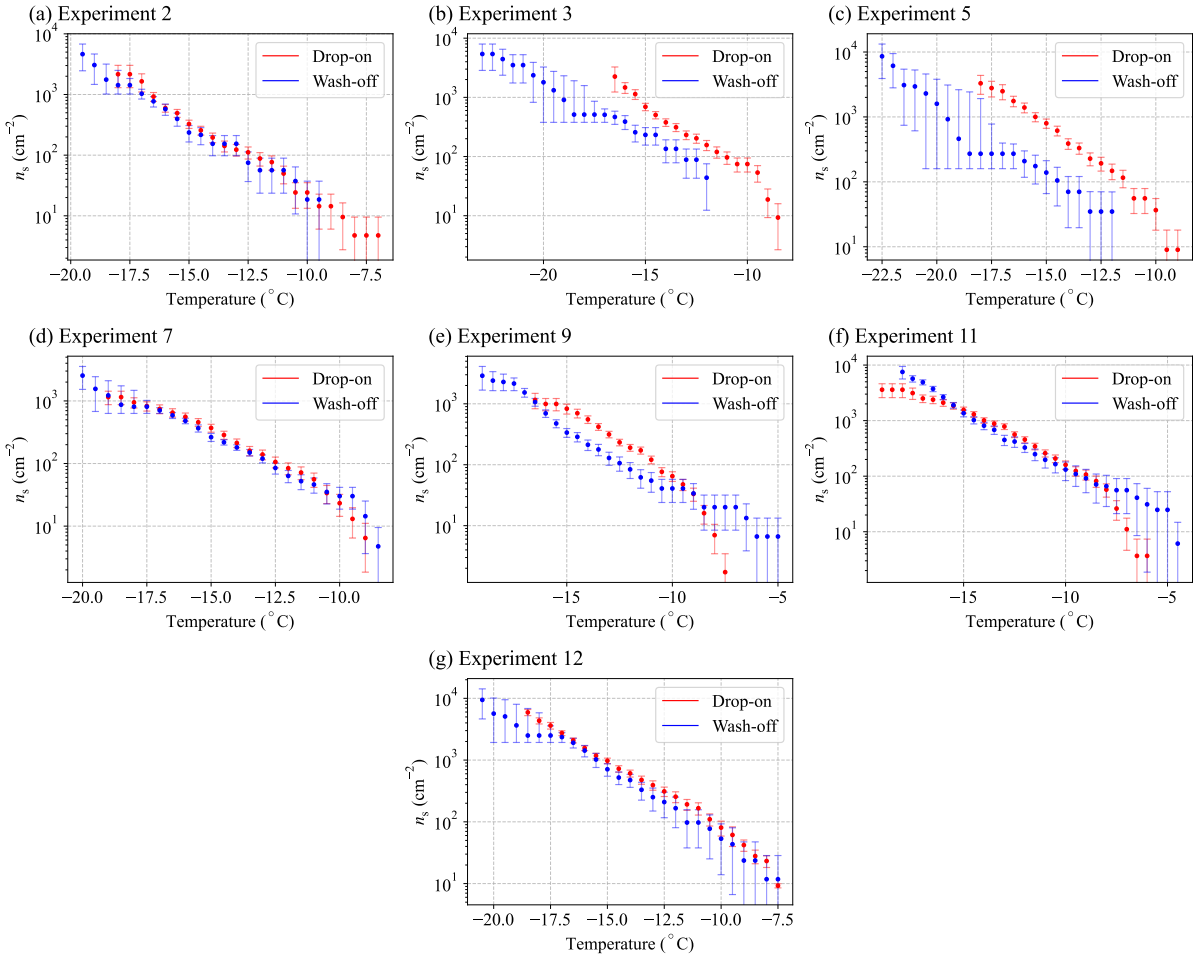

Figure S4: Active site density with error bars for all Copper River dust experiments.

Table S3: Information about Agricultural Soil Dust Experiments.

ID	Date	Volume (L^{-1})	Number Conc. (cm^{-3})	Number Conc. σ (cm^{-3})	Surface Area ($\mu m^2 cm^{-3}$)	Surface Area σ ($\mu m^2 cm^{-3}$)	Peak Diameter (μm)
22	20/03/24	610	170.41	104.66	151.53	63.91	0.8
23	21/03/24	320	22.20	28.14	16.81	14.29	0.7
24	22/03/24	600	282.95	123.33	271.83	63.80	0.8
27	02/05/24	600	28.66	34.16	16.72	13.87	0.7
28	02/05/24	600	75.67	56.01	47.96	20.30	0.7
29	03/05/24	600	62.83	50.17	42.54	19.83	0.8

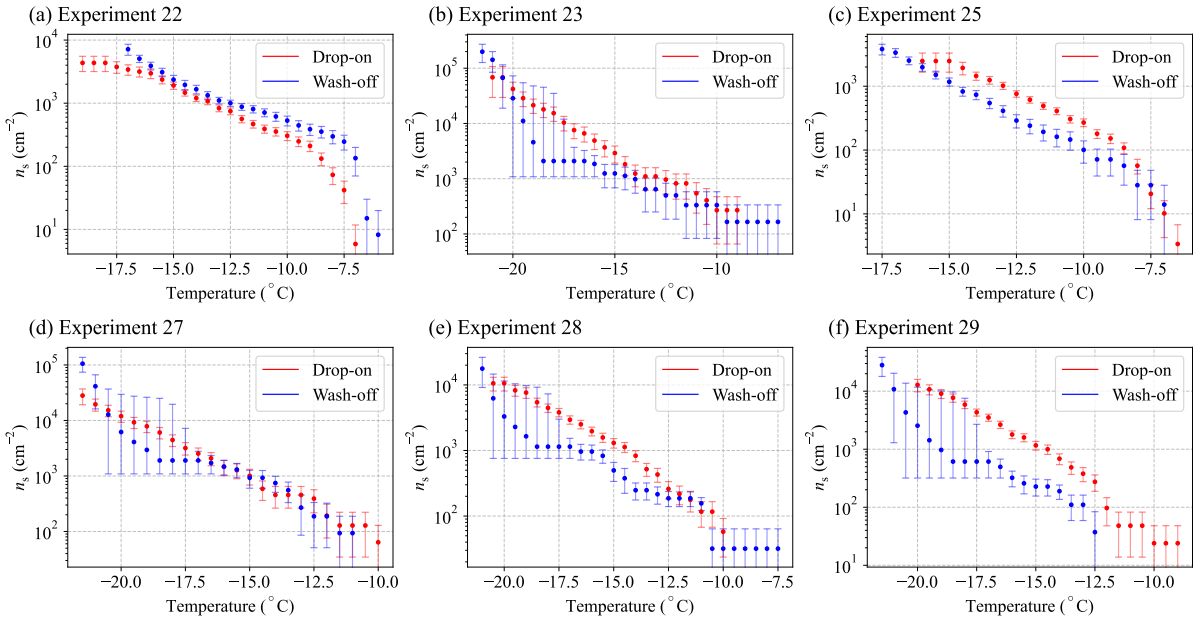

Figure S5: Active site density with error bars for all Agricultural Soil Dust experiments.

S2.2 Wet-Dispersed Samples

Table S4: Information about Snomax Filtrate Experiments.

ID	Date	Volume (L^{-1})	Number Conc. (cm^{-3})	Number Conc. σ (cm^{-3})	Surface Area ($\mu m^2 cm^{-3}$)	Surface Area σ ($\mu m^2 cm^{-3}$)	Peak Diameter (μm)
40	17/05/24	600	894.90	1051.84	100.86	170.56	0.3
42	20/05/24	600	2611.33	2471.45	239.98	224.56	0.25
43	20/05/24	300	3198.33	1900.62	278.27	158.09	0.25
44	21/05/24	451.7	908.61	613.41	66.44	50.93	0.25
69[1]	02/05/25	N/A	N/A	N/A	N/A	N/A	N/A

[1]PINE experiment only

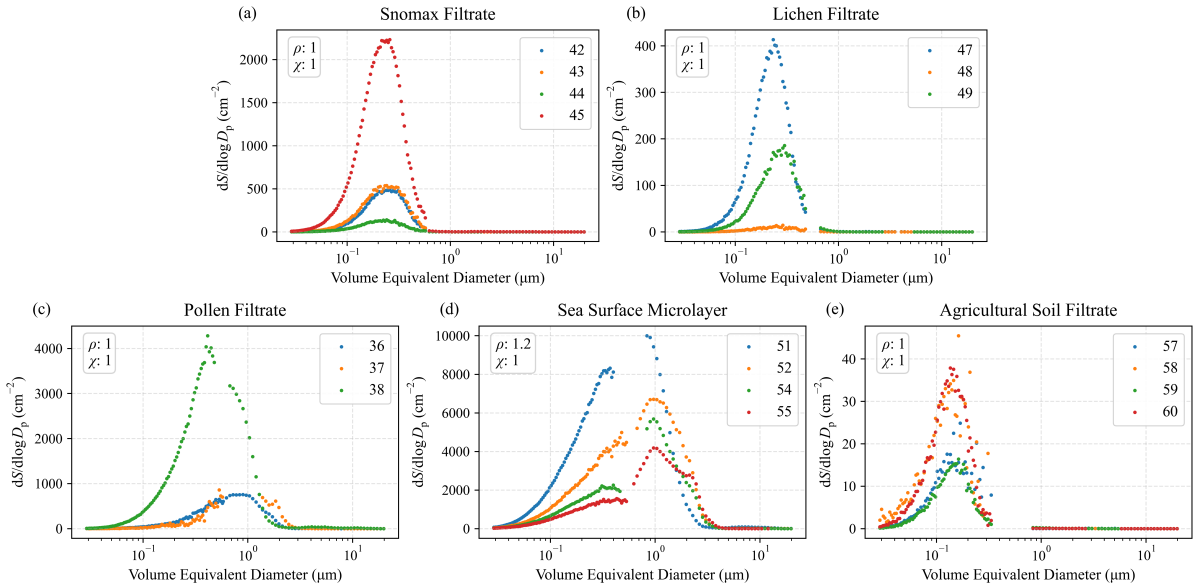

Figure S6: $\frac{\mathrm{d}S}{\mathrm{d}\log D_\mathrm{p}}$ size distributions for wet-dispersed samples from both the APS and SMPS data averaged over the experiment. The filtrate materials all peak in the accumulation mode. The sea surface microlayer was not filtered and contains some larger particles.

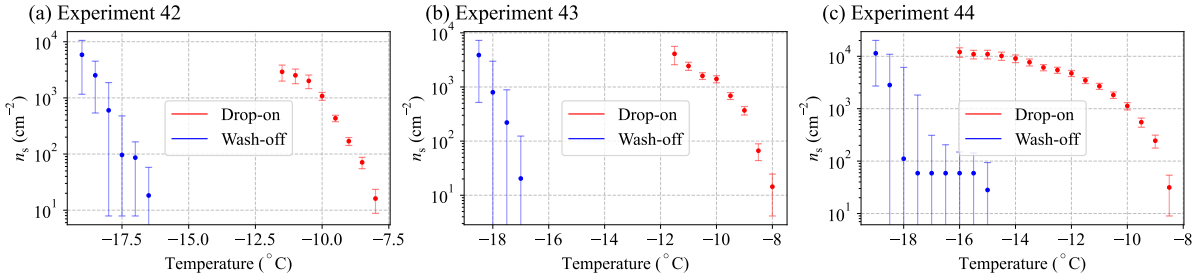

Figure S7: Active site density with error bars for all Snomax Filtrate experiments.

Table S5: Information about Lichen Filtrate Experiments.

ID	Date	Volume (L^{-1})	Number Conc. (cm^{-3})	Number Conc. σ (cm^{-3})	Surface Area ($\mu m^2 cm^{-3}$)	Surface Area σ ($\mu m^2 cm^{-3}$)	Peak Diameter (μm)
47	24/05/24	600	1807.33	1638.94	169.07	144.98	0.2
48	24/05/24	600	53.93	66.98	5.50	7.97	0.2
49	24/05/24	600	669.33	318.12	80.73	37.26	0.3

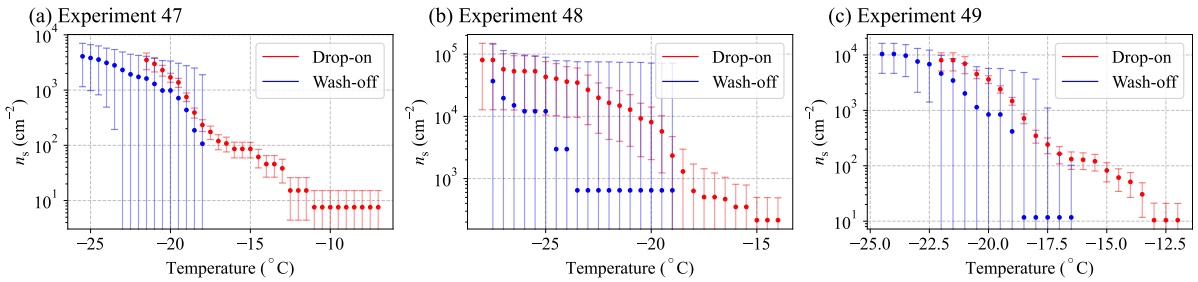

Figure S8: Active site density with error bars for all Lichen Filtrate experiments.

Table S6: Information about Pollen Filtrate Experiments.

ID	Date	Volume (L^{-1})	Number Conc. (cm^{-3})	Number Conc. σ (cm^{-3})	Surface Area ($\mu m^2 cm^{-3}$)	Surface Area σ ($\mu m^2 cm^{-3}$)	Peak Diameter (μm)
36	14/05/24	250	1426.80	652.09	515.75	218.73	0.9
37	15/05/24	600	982.16	1569.88	540.53	600.25	0.9
38	15/05/24	600	11996.02	7238.38	2632.95	1380.14	0.4

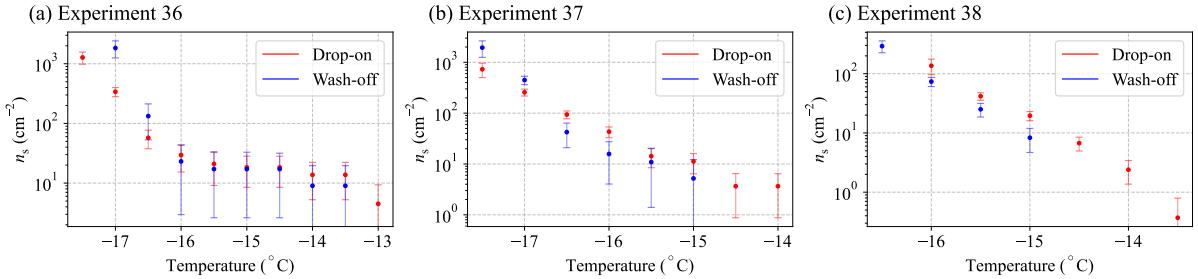

Figure S9: Active site density with error bars for all Pollen Filtrate experiments.

Table S7: Information about Sea Surface Microlayer Experiments.

ID	Date	Volume (L^{-1})	Number Conc. (cm^{-3})	Number Conc. σ (cm^{-3})	Surface Area ($\mu m^2 cm^{-3}$)	Surface Area σ ($\mu m^2 cm^{-3}$)	Peak Diameter (μm)
51	14/08/24	600	60876.39	32366.40	8956.88	3908.88	0.7
52	14/08/24	600	30485.23	19699.20	6001.87	3632.29	1
54	16/08/24	700	19304.24	11988.92	3987.13	2556.94	1
55	16/08/24	300	14287.07	5318.37	3174.25	1384.00	1

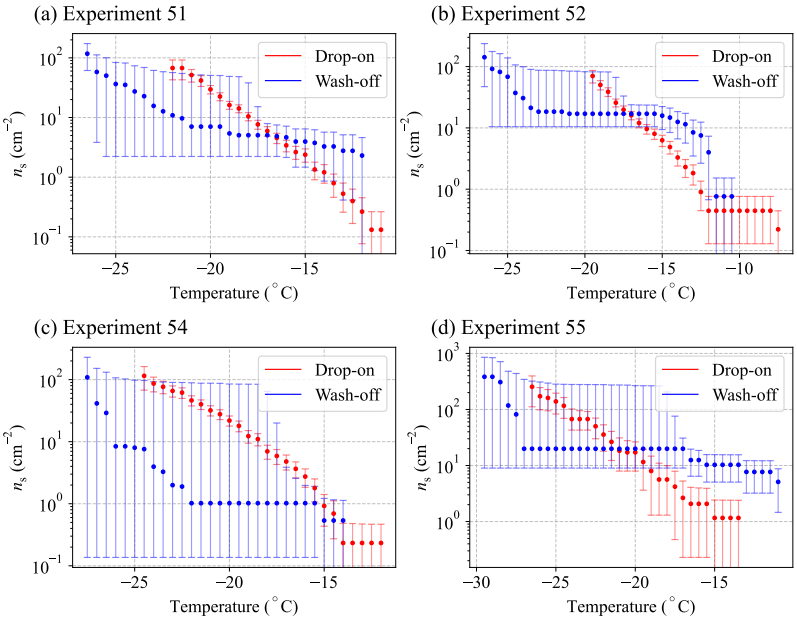

Figure S10: Active site density with error bars for all sea surface microlayer experiments.

Table S8: Information about Agricultural Soil Filtrate Experiments.

ID	Date	Volume (L^{-1})	Number Conc. (cm^{-3})	Number Conc. σ (cm^{-3})	Surface Area ($\mu m^2 cm^{-3}$)	Surface Area σ ($\mu m^2 cm^{-3}$)	Peak Diameter (μm)
57	20/08/24	600	219.26	279.02	10.66	21.06	0.15
58	21/08/24	600	607.92	1016.28	19.92	35.61	0.15
59	21/08/24	900	70.87	159.43	6.71	7.07	0.15
60	21/08/24	300	460.45	242.80	15.95	9.57	0.15

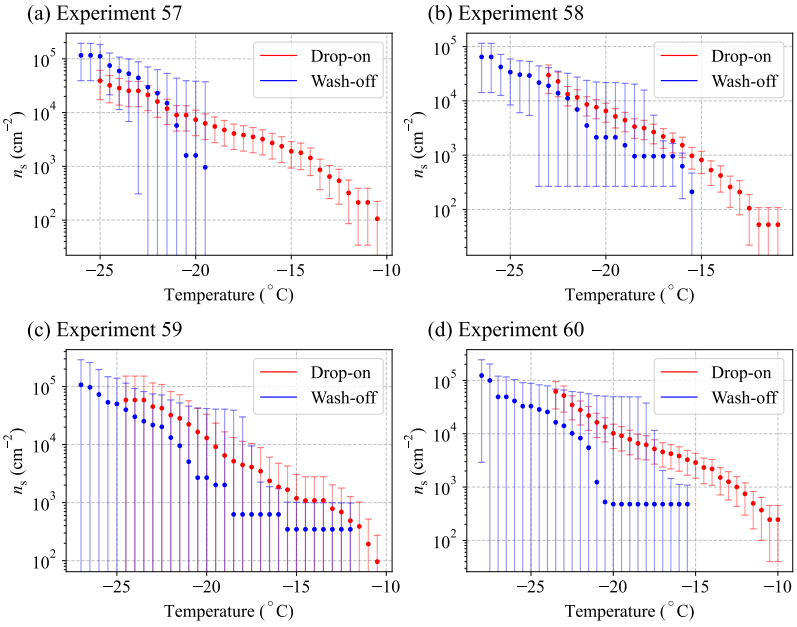

Figure S11: Active site density with error bars for all Soil Filtrate experiments.

Material	χ	ρ	Source
Copper River Dust	1.3	2.6	Möhler et al. [2008]
Agricultural Soil Dust	1.3	2.6	Möhler et al. [2008]
Lichen Filtrate	1	1	Experimentally Determined
Agricultural Soil Filtrate	1	1	Experimentally Determined
Snomax Filtrate	1	1	Experimentally Determined
Sea Surface Microlayer	1	1.2	Experimentally Determined
Pollen Filtrate	1	1	Experimentally Determined
Dry Snomax	1.1	1.35	Wex et al. [2015]

Table S9: Dynamic shape factor (χ) and density (ρ) for each material in this study.

S3 Merging Particle Size Distributions

Particle size distributions were measured using a TSI Aerodynamic Particle Sizer (APS) and Scanning Mobility Particle Sizer (SMPS). The APS measures particles predominantly in the coarse mode (0.523 to 19.81 μm), while the SMPS measures primarily in the accumulation mode (0.0146 to 0.6854 μm), enabling measurements across three orders of magnitude. To merge the two datasets, both instrument diameters were converted to volume-equivalent diameters. The APS aerodynamic diameter was converted using the APS factor, F_{APS}, in Equation S1, while the SMPS electrostatic diameter was converted using the SMPS factor, F_{SMPS}, in Equation S2 [Möhler et al., 2008].

$$F_{APS} = \sqrt{\frac{\chi}{\rho}} \tag{S1}$$

$$F_{SMPS} = \frac{1}{\chi} \tag{S2}$$

Where χ is the dynamic shape factor, reflecting how spherical the particles are, and ρ is the particle density (g cm^{-3}). χ and ρ values used for each material are listed in Table S9. Some values were taken directly from the literature, where available. In other cases, we chose values that produced consistency between the APS and SMPS data and were physically reasonable (for example, nebulised aqueous aerosol is expected to have a shape factor of around 1). For each experiment, the largest SMPS bins and smallest APS bins were removed as these bins are known to undercount. These processed volume median size distributions (Figure S2 and Figure S6) were then used to compute the total surface area (in Table S2 to Table S8). To determine the uncertainty in the total surface area, the error is propagated from the raw files. In the raw files, the number of particles detected in each bin is used to calculate the Poisson counting uncertainty. The percent error is then calculated and propagated through to the final total surface area value.

S4 PINE Pressure Bins

In standard PINE data analysis, each expansion yields a single data point, where the temperature corresponds to the condition reached after expanding to a defined pressure. This produces a single cumulative ice-nucleating particle concentration at the lowest temperature of the expansion. This approach works well in cases where the INP concentration is very low, such as ambient aerosol, because only a small number of INPs are detected over the course of the expansion. However, in these laboratory experiments, the aerosol concentration is sufficiently

high that a large number of particles activate to ice during a single expansion. Under these conditions, we can bin the data through an expansion to produce cumulative INP concentrations over a range of temperatures. We divided each expansion into five equal-sized pressure bins. For example, a 1000-750 hPa expansion yields the following bins: 1000-950 hPa, 950-900 hPa, 900-850 hPa, 850-800 hPa, and 800-750 hPa. The lowest temperature for each bin was estimated assuming adiabatic expansion, and INP concentration was calculated from the number of ice crystals detected within each bin and the volume of gas passing through the detection volume (at standard temperature and pressure).

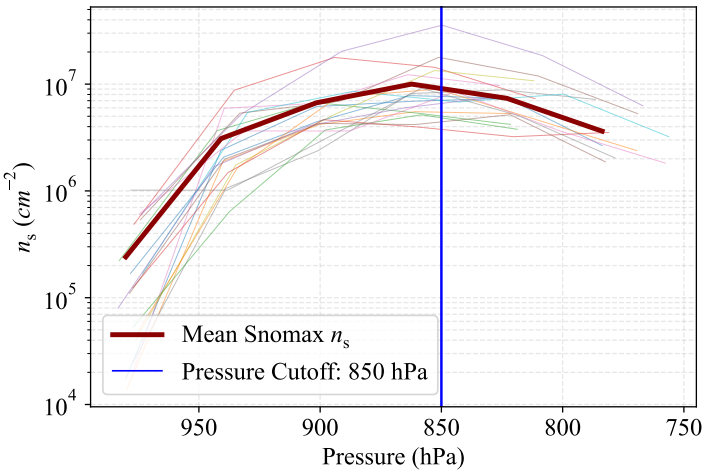

Figure S12: $n_s(T)$ vs pressure for all the dry Snomax experiments. The decrease in activity below 850 hPa is associated with the loss of ice crystals during the later stages of the expansion. This behaviour motivates the selection of 850 hPa as the lower pressure cutoff used throughout the PINE dataset.

By definition, $N_{INP}(T)$ is cumulative and therefore must increase (or stay constant) with decreasing temperature. However, when ice crystals grow during expansion, they can be lost from the chamber through sedimentation or impaction, leading to an apparent decrease in the measured cumulative INP concentration. In some experiments, we noted a decrease in $N_{INP}(T)$ in the lower temperature (pressure) bins, which is consistent with the loss of ice crystals from the chamber during the later stages of the expansion. To determine an appropriate lower pressure cutoff, we analysed the dry Snomax experiments, for which the ice-nucleating behaviour is well-characterised. In these experiments, $N_{INP}(T)$ is expected to increase sharply with decreasing temperature and then plateau [Wex et al., 2015]. If no ice crystals were lost in an expansion, this same increase should be observed at higher pressures, followed by a plateau in the lower pressure bins. However, in our PINE data, the $n_s(T)$ reaches a maximum at approximately 850 hPa and subsequently decreases slightly at lower pressures (Figure S12). This behaviour indicates that the ice crystal losses become significant below this pressure cutoff, rendering the data unreliable. Based on this consistent feature across the dry Snomax PINE experiments, we define 850 hPa as the minimum reliable pressure for all PINE experiments and exclude all pressure bins below this threshold in our analysis. This approach removes the low bias introduced by ice crystal loss. The dry Snomax PINE data with the 850 hPa pressure cutoff can be seen in Figure S12.

References

O. Möhler, S. Benz, H. Saathoff, M. Schnaiter, R. Wagner, J. Schneider, S. Walter, V. Ebert, and S. Wagner. The effect of organic coating on the heterogeneous ice nucleation efficiency of mineral dust

aerosols. *Environmental Research Letters*, 3(2), 6 2008. ISSN 17489326. doi: 10.1088/1748-9326/3/2/025007.

H. Wex, S. Augustin-Bauditz, Y. Boose, C. Budke, J. Curtius, K. Diehl, A. Dreyer, F. Frank, S. Hartmann, N. Hiranuma, E. Jantsch, Z. A. Kanji, A. Kiselev, T. Koop, O. Möhler, D. Niedermeier, B. Nillius, M. Rösch, D. Rose, C. Schmidt, I. Steinke, and F. Stratmann. Intercomparing different devices for the investigation of ice nucleating particles using Snomax® as test substance. *Atmospheric Chemistry and Physics*, 15(3):1463–1485, 2 2015. ISSN 16807324. doi: 10.5194/acp-15-1463-2015.